

Ligand- and Structure-Based Virtual Screening for Clathroдин-Derived Human Voltage-Gated Sodium Channel Modulators

Tihomir Tomašić,[†] Basil Hartzoulakis,[‡] Nace Zidar,[†] Fiona Chan,[‡] Robert W. Kirby,[‡] David J. Madge,[‡] Steve Peigneur,[§] Jan Tytgat,[§] and Danijel Kikelj^{†,*}

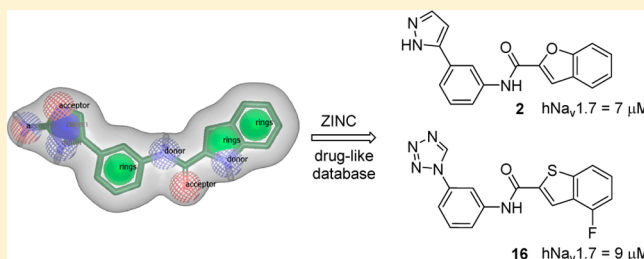
[†]University of Ljubljana, Faculty of Pharmacy, Aškerčeva 7, 1000 Ljubljana, Slovenia

[‡]Xention Limited, Iconix Park, London Road, Pampisford, Cambridge CB22 3EG, United Kingdom

[§]University of Leuven (K. U. Leuven), Toxicology and Pharmacology, Campus Gasthuisberg O&N2, Herestraat 49, P.O. Box 922, 3000 Leuven, Belgium

S Supporting Information

ABSTRACT: Voltage-gated sodium channels (VGSC) are attractive targets for drug discovery because of the broad therapeutic potential of their modulators. On the basis of the structure of marine alkaloid clathroдин, we have recently discovered novel subtype-selective VGSC modulators I and II that were used as starting points for two different ligand-based virtual screening approaches for discovery of novel VGSC modulators. Similarity searching in the ZINC database of drug-like compounds based on compound I resulted in five state-dependent $\text{Na}_v1.3$ and $\text{Na}_v1.7$ modulators with improved activity compared to I ($\text{IC}_{50} < 20 \mu\text{M}$). Compounds 2 and 16 that blocked sodium permeation in $\text{Na}_v1.7$ with IC_{50} values of 7 and 9 μM , respectively, are among the most potent clathroдин analogs discovered so far. In the case of compound II, 3D similarity searching in the same database was followed by docking of an enriched compound library into our human $\text{Na}_v1.4$ open-pore homology model. Although some of the selected compounds, e.g., 31 and 32 displayed 21% and 22% inactivated state I_{peak} block of $\text{Na}_v1.4$ at 10 μM , respectively, none showed better $\text{Na}_v1.4$ modulatory activity than compound II. Taken together, virtual screening yielded compounds 2 and 16, which represent novel scaffolds for the discovery of human $\text{Na}_v1.7$ modulators.



INTRODUCTION

Voltage-gated sodium channels (VGSC) are complex membrane proteins playing a key role in the initiation and propagation of action potentials in neurons and other electrically excitable cells such as myocytes and endocrine cells.¹ They activate in response to membrane depolarization and are responsible for the rapid influx of sodium ions during the rising phase of the action potential. During this process, VGSC activate and inactivate within milliseconds. VGSC are a family of heteromeric protein complexes consisting of four homologous domains (DI–DIV) of six transmembrane segments (S1–S6) constituting a pore-forming α -subunit, which is in association with one or more β -subunits.² The aqueous ion-conducting pore is positioned at the extracellular side of the cell membrane and is formed by S5 and S6 helices of the four domains, linked by P-loops that fold partly back into the membrane to form the outer vestibule.^{2,3} The latter hosts the selectivity filter (DEKA motif), which comprises four different amino acid side chains, one from each domain: Asp (DI), Glu (DII), Lys (DIII), and Ala (DIV).

VGSC participate in many physiological processes including nociception, locomotion, and cognition. Nine different α subunits ($\text{Na}_v1.1$ – $\text{Na}_v1.9$) have been identified, which show distinct expression patterns in various parts of the peripheral

and central nervous system (CNS) and in muscle cells.⁴ Isoforms $\text{Na}_v1.1$ – 1.3 and $\text{Na}_v1.6$ are mainly expressed in CNS, $\text{Na}_v1.4$ in skeletal muscle, and $\text{Na}_v1.5$ in the heart, while $\text{Na}_v1.7$ – 1.9 are characteristic of sensory neurons.⁵ These isoforms possess a high degree of sequence similarity, which translates into their similar pharmacological properties. Many pharmacological and genetic studies have revealed an important role of single VGSC subtypes in various disorders (channelopathies). Mutations in VGSC genes responsible for channelopathies have been found in brain, heart, and peripheral nerves and skeletal muscle.⁶ Disturbances in activity of $\text{Na}_v1.1$ or $\text{Na}_v1.2$ can lead to epilepsy^{7,8} and Dravet syndrome,⁹ whereas $\text{Na}_v1.3$ and $\text{Na}_v1.7$ – 1.9 subtype disorders are involved in neuropathic pain.¹⁰ Mutations in $\text{Na}_v1.4$ that result in hyperactivity of skeletal sodium channels are responsible for paralysis¹¹ and myotonia,¹² while cardiac channelopathies, such as Brugada syndrome,¹³ long QT syndrome,¹⁴ and atrial fibrillation,¹⁵ are associated with altered $\text{Na}_v1.5$ function. As a result of the broad therapeutic potential of VGSC modulators, discovery of drugs targeting VGSC has received a high degree of interest from the pharmaceutical industry.^{16–18} Currently,

Received: August 29, 2013

Published: November 11, 2013

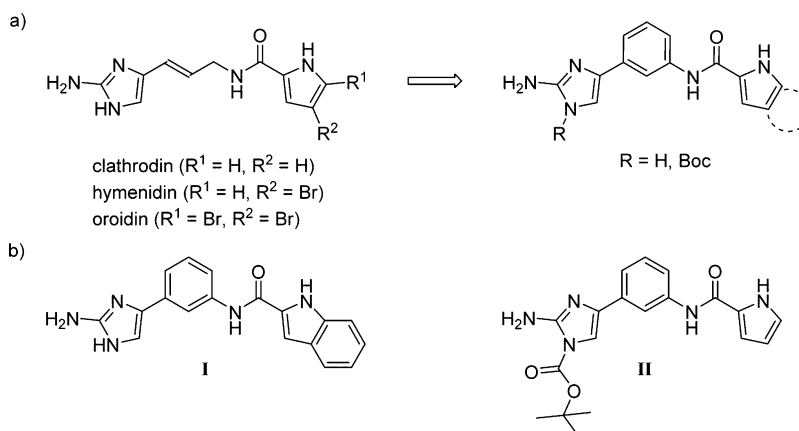


Figure 1. Pyrrole-imidazole alkaloids, clathrocin, hymenidin, and oroidin, from *Agelas* sponges and their structural modification (a) leading to the novel VGSC modulators **I** and **II** (b).

marketed drugs targeting voltage-gated sodium channels include local anesthetics (LA), antiarrhythmics, and anti-convulsants, which provide good clinical efficacy by blockade of VGSC. However, most of them show weak affinity and poor selectivity among channel subtypes, which has led to increasing efforts to identify subtype-selective modulators that might be expected to possess improved clinical efficacy and reduced side-effect profile.¹⁹ Although clinically useful sodium channel modulators display low subtype selectivity, most of them possess relatively favorable side-effect profiles, which is generally attributed to their state-dependent action. LA have low affinity for VGSC in the resting state and much higher affinity for channels in the open or inactivated states. LA also exhibit a use-dependent block of VGSC because they have little effect on the channels firing at a slow rate but block the channels to a greater extent when they are firing with high-frequency, which is common under pathological conditions.²⁰ Therefore, in the discovery of novel VGSC modulators, the researchers can focus either on the development of potent isoform-selective VGSC modulators^{21–23} or on the design of broad spectrum VGSC blockers with a greater level of state dependence.²⁴ Because cardiac risk is associated with off-target effects of sodium channel modulators on the $Na_v1.5$ isoform, selectivity against this channel is of paramount importance in the profile of novel sodium channel modulators.¹⁹

The potential of structure-based design in the discovery of novel VGSC modulators has recently increased after determination of the first crystal structures of the bacterial voltage-gated sodium channels in their closed^{3,25,26} and open²⁷ states, which enable building of homology models of different human VGSC isoforms. In the past, homology models of VGSC were mostly based on the crystal structures of bacterial voltage-gated potassium channels and were extensively used in studies of toxin and local anesthetic binding to the pore of the channel.²⁸ However, examples of using a homology model in virtual screening for potential voltage-gated ion channel modulators are rare.²⁹

The marine ecosystem is a rich source of structurally diverse toxins, e.g., tetrodotoxin (TTX), saxitoxin, and μ -conotoxin, that display activity on VGSC.³⁰ Also pyrrole-imidazole alkaloids,^{31,32} clathrocin, oroidin, and hymenidin (Figure 1a) from the Caribbean sponges of the genus *Agelas* have shown modulatory activities on the voltage-gated sodium³³ and calcium³⁴ channels. In cells isolated from chick embryo

sympathetic ganglia, clathrocin acted as a VGSC modulator by influencing channel ionic conduction.³³

We have recently started to explore the potential of clathrocin analogs for blocking different VGSC isoforms.^{35,36} Systematic structural modification of clathrocin (Figure 1a) led us to compound **I** that possessed $Na_v1.3$ and $Na_v1.7$ blocking activity (IC_{50} values of 21 and 25 μM for free base, respectively) and **II** that displayed an inactivated state $Na_v1.4$ I_{peak} block of 68% at 10 μM (Figure 1b). In the present work, these two clathrocin analogs were used in the ligand-based virtual screening using the ROCS (OpenEye Scientific Software, Inc.)³⁷ method of molecular shape comparison to obtain an enriched subset of the ZINC library of commercially available screening compounds (Figure 2).³⁸ In the case of

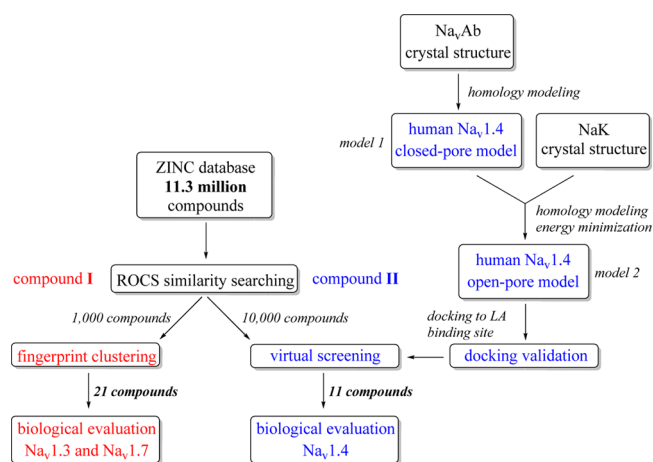


Figure 2. Overview of the virtual screening workflow used in the present study.

compound **II**, a subset of compounds resulting from ROCS search was further used for structure-based virtual screening in a homology model of human $Na_v1.4$ in its open-pore conformation, which we built as part of this work, on the basis of a recently published first crystal structure of VGSC³ (Figure 2). Altogether, after inspection of hits from both virtual screening campaigns, 32 compounds were purchased and electrophysiologically evaluated. Twenty-one compounds from the first series were screened for their modulatory activity on human $Na_v1.3$, $Na_v1.5$, and $Na_v1.7$ isoforms, and 11

compounds from the second series were tested on the Na_v1.4 isoform. This resulted in the discovery of novel VGSC modulators, **2**, **5**, and **16**, originally based on the marine alkaloid clathrocin.

■ EXPERIMENTAL SECTION

Computer Hardware. All of the computational work was performed on two workstations. Accelrys Discovery Studio 3.0 (DS)³⁹ is running on a workstation with an Intel core i7 860 CPU processor, 8 GB RAM, two 750 GB hard drives and a Nvidia GT220 GPU graphic card, running Centos 5.5. LeadIT (version 2.1.2.),⁴⁰ and OpenEye Scientific Software is running on four octal core AMD Opteron CPU processors, 16 GB RAM, two 750 GB hard drives, running 64-bit Scientific Linux 6.0.

Compound Database Preparation. A drug-like subset of the ZINC³⁸ database of commercially available compounds was downloaded, and the bank of 11.3 million compounds was prepared with OMEGA (OpenEye Scientific Software, Inc.)⁴¹ to provide an average of 152 conformations per compound.

3D Similarity Search. In the ligand-based virtual screening for structurally similar compounds to **I** and **II** in the prepared ZINC bank of drug-like compounds (Figure 2),³⁸ 3D similarity searching was implemented in ROCS (OpenEye Scientific Software, Inc.)³⁷ using compound **I** or **II** as a query (Figure S1, Supporting Information). In both cases, hits were ranked according to their TanimotoCombo score, which considers molecular shape (shape score) and atom type (color score) similarities.

In the case of ROCS similarity searching using compound **I** as a query, a set of 1000 compounds with the highest TanimotoCombo score was clustered according to their functional-class fingerprints (FCFP-6) using the Cluster Ligands protocol in DS (Figure 2). Twenty one compounds were selected based on their TanimotoCombo score and structural diversity between them and were purchased from Enamine Ltd.

In the case of the second ROCS 3D similarity searching based on compound **II**, a set of 10,000 compounds with the highest TanimotoCombo score was retained. This enriched bank of compounds was used as an input for docking to our human Na_v1.4 open-pore conformation homology model (Figure 2).

Homology Modeling. **1. Closed-Pore Conformation Model of Human Na_v1.4 (Model 1).** Our closed-pore conformation human Na_v1.4 homology model was built based on the first crystal structure of VGSC from bacterium *Arcobacter butzleri* (Na_vAb)³ (Figure S4, Supporting Information). Sequence alignment of human Na_v1.4 and Na_vAb is presented in Figure S2 of the Supporting Information. P-loop residues of human Na_v1.4 and Na_vAb were aligned as proposed by Tikhonov and Zhorov⁴² by including gaps in the human Na_v1.4 sequence at positions where point deletions probably occurred during evolution. Extracellular P-loops between S5 and S6 helices of human Na_v1.4 are considerably longer when compared to those of Na_vAb. Hence, P-loops were shortened to the region that could be modeled based on the template structure of Na_vAb (Figure S2, Supporting Information).

The described sequence alignment (Figure S2, Supporting Information) was used as an input for building a closed-pore homology model of human Na_v1.4 based on the Na_vAb crystal structure (PDB entry: 3RVY) (Figure S4, Supporting Information). Homology modeling was performed with Build

Homology Models protocol in DS, which is based on the MODELLER⁴³ software. Optimization Level was set to high, while the Refine Loops parameter was set to false. One hundred models of the S4–S6 part of each domain (DI–IV) were generated, and the model with the highest discrete optimized protein energy (DOPE) score and best Protein Health Report (obtained with the Check Structure tool in DS), as well as conformational similarity to the template was selected. All four domain models were superimposed with the template structure to obtain a heterotetrameric homology model of S4–S6 part of human Na_v1.4 in the closed-pore conformation (model 1). It has to be noted here that domains I–IV of the model are not connected because there are no suitable templates available for modeling of the intracellular loops of human VGSC.

2. Open-Pore Conformation Model of Human Na_v1.4 (Model 2). The nonselective cation channel NaK from *Bacillus cereus* for which the three-dimensional structures of the closed-pore (PDB entry: 2AHY)⁴⁴ and open-pore (PDB entry: 3E86)⁴⁵ conformations are known (Figure S5, Supporting Information) was used as a template for building of the open-pore conformation homology model of human Na_v1.4. Superimposition of the closed- and open-pore conformations of NaK revealed that major structural differences seem to occur in the pore-lining inner helices below the selectivity filter, while regions surrounding the selectivity filter are almost identical⁴⁵ (Figures S5 and S6, Supporting Information). Because regions surrounding the selectivity filter (residues 35 to 85 in NaK channel) seem to remain static during channel gating,⁴⁵ we retained conformation of S5 helices and P-loops from model 1. In contrast, major conformational changes can be observed in S6 helices (Figure S6, Supporting Information). Thus, the S6 helices of model 1 were replaced by those that were modeled based on the open-pore conformation of NaK channel (PDB entry: 3E86), according to the sequence alignment presented in Figure S3 of the Supporting Information (initial model 2). The opening of VGSC is also accompanied with conformational changes of the voltage sensor S4.⁴⁶ In our open-pore homology model of human Na_v1.4, based on the Na_vAb and NaK as templates, there is an overlap between the S4 helices of the model 1 and the S6 helices of the initial model 2 because the conformational changes in S4 were not modeled due to the absence of the voltage sensor in NaK open-pore structure. Hence, the S4 helices of initial model 2 were deleted, which resulted in the S5–S6 part (ion-conducting pore) of the Na_v1.4 (model 2).

3. Energy Minimization. **3.1. Placing the Channel in the Lipid Environment.** The protein was first typed with CHARMm⁴⁷ force field. Add Membrane and Orient Molecule protocol in DS, which uses CHARMm solvation models to optimize the location of molecule with respect to membrane, was used to place the protein in the implicit membrane model. The thickness of the membrane was set to 25 Å. After addition of the membrane, the position of the protein was optimized manually.

3.2. Energy Minimization. The backbone atoms of the protein were restrained using the Create Harmonic Restraint tool in DS. The force constant was set to 250 kcal/(mol Å²), mass weighting was allowed, and absolute harmonic restraint type was used. The protein was minimized using 1000 steps of the steepest descent algorithm, followed by 1000 steps of the conjugate gradients minimization. The RMS gradient tolerance was set to 0.001 (kcal/mol Å) with energy change set to 0.0.

Generalized Born with Implicit Membrane (GBIM) was used as the implicit solvent model. GBIM includes implicit membrane in the calculations of the electrostatic contribution to solvation energy. The nonpolar region of the membrane is approximated as a planar dielectric slab having the same dielectric constant as inside the molecule.⁴⁸ The dielectric constant was set to 1, and the implicit solvent dielectric constant was set to 80. The distance cutoff value was set to 14 Å to use for counting nonbonded interaction pairs. The energy minimized structure was evaluated for its geometrical quality using Procheck.⁴⁹

4. Model Validation by Molecular Docking. **4.1. Ligand Preparation.** TTX and local anesthetic etidocaine were used as probes to explore whether the known experimental data on their binding could be reproduced by docking into our open-pore conformation homology model of human Na_v1.4. The three-dimensional models of TTX and etidocaine (Figure S9, Supporting Information) were built from a standard fragment library in DS. The geometries of the molecules were optimized using CHARMM⁴⁷ force field with MMFF94⁵⁰ partial atomic charges and the energy was minimized using the Smart Minimizer algorithm in DS until the gradient value was smaller than 0.001 kcal/(mol Å).

4.2. Model and Docking Protocol Validation. FlexX,^{51,52} as available in LeadIt,⁴⁰ was used for molecular docking. Receptor was prepared in LeadIT graphical user interface using the Receptor wizard. For docking of TTX, amino acid residues within a radius of 10 Å around the DEKA motif (Asp406, Glu761, Lys1244, Ala1536) were defined as the binding site. For docking of etidocaine, amino acid residues within a radius of 10 Å around the amino acids interacting with LA (Leu1287, Phe1586, and Tyr1593) were defined as the binding site. Hydrogen atoms were added to the binding site residues, and correct tautomers and protonation states were assigned. Triangle matching was used to place the “base fragment”. The maximum number of solutions per iteration and the maximum number of solutions per fragmentation parameter values were increased to 500, while other parameters were set at their default values.

Virtual Screening. In the structure-based virtual screening for potential Na_v1.4 modulators among 10,000 similar compounds to compound II (Figure 2), FlexX was used for molecular docking of compounds into the inner pore of the energy-minimized human Na_v1.4 open-pore conformation homology model. From the electrophysiology data, it can be anticipated that compound II binds to the LA binding site in the inner pore of the channel. Receptor and docking parameters were used as described above for docking of etidocaine. All 10,000 compounds were docked into the defined binding site and ranked according to the score of the best ranked conformation. From the highest ranked compounds, 11 were selected and purchased from Enamine Ltd.

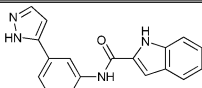
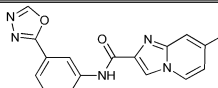
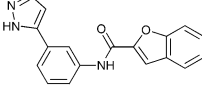
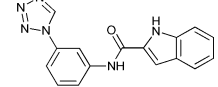
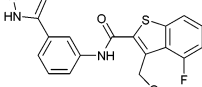
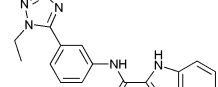
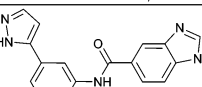
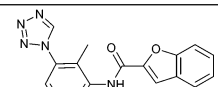
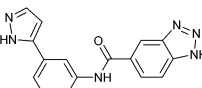
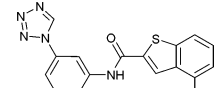
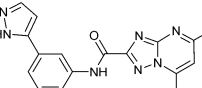
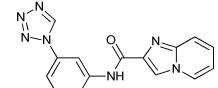
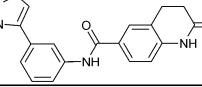
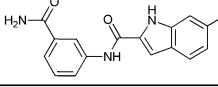
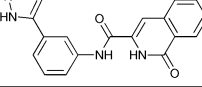
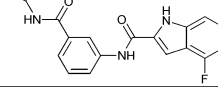
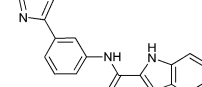
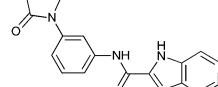
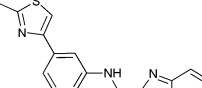
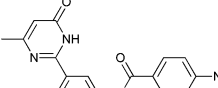
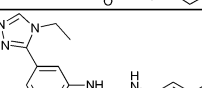
Electrophysiology. **1. Patch Clamp.** Cells were prepared by dissociation from T175 cell culture flasks using trypsin-EDTA (0.05%), and cells were kept in serum-free media in the cell hotel on board the QPatch HT. These cells were sampled, washed, and resuspended in extracellular recording solution by the QPatch HT immediately before application to well site on the chip. Once in whole-cell configuration, the vehicle (0.1% DMSO v/v) was applied to the cells to achieve a stable control recording (4 min total). For potency (IC₅₀) testing, the vehicle control period was followed by application of test concentrations as a single bolus addition (4 min incubation per test

concentration). For single-concentration efficacy testing, the vehicle control period was followed by a 10 min recording period during where two bolus applications of the test compound (10 μM) were applied to the cells at 5 min intervals. Compounds were prepared in extracellular recording solution from a 10 mM (100% DMSO) stock to yield a final 10 μM (0.1% DMSO) test concentration, and for dose dependent studies, subsequent serial dilutions in extracellular solution were performed (0.3–10 μM). Currents were elicited from Na_v1.3, Na_v1.4, and Na_v1.7 cell lines using a standard two-pulse voltage protocol. From a holding potential of −100 mV, a 20 ms activating step to −20 mV was applied to assess the effect of compounds on resting (closed) state block. The second activating pulse was applied following a 5 s prepulse to half inactivation potential (variable depending on the sodium channel studied, −65 to −75 mV) to assess block on the open-inactivated state of the channel. This protocol was applied at a sweep interval of 0.067 Hz throughout the duration of the experiment. To study Na_v1.5 currents, a pulse train consisting of 10 repetitive activating test pulses to −20 mV from a holding potential of −100 mV were applied at a 1 Hz frequency until 10 pulses were reached, this sequence was repeated at a sweep interval of 0.016 Hz throughout the duration of the experiment. For Na_v1.3, Na_v1.4, and Na_v1.7 channels, the peak inward current was determined for both the closed and open-inactivated test pulses recorded from each sweep applied to the cells and for Na_v1.5 from the tenth pulse of each pulse train recorded. Data was captured using QPatch assay software (v5.0). The % inhibition of inactivated-state peak current (*I*_{peak}) was calculated as the mean peak current value for the last three sweeps measured in each concentration test period relative to the last three sweeps recorded during the control vehicle period. Sigmoidal concentration response curves (four parameter logistic curve) were fitted to the % inhibition data using Xlfit (IDBS) from which the IC₅₀ was determined. Fits were constrained at 0 and 100%. Data are presented as mean ± SD for minimum of 3 independent observations.

2. Two-Electrode Voltage Clamp. **2.1. Heterologous Expression.** For expression in *Xenopus laevis* oocytes, Na_v1.3/pLCT2 (*NotI*), Na_v1.4/pUI-2 (*NotI*), Na_v1.7/pBSTA.rPN1 (*SacII*), and hβ1/pGEM-HE (*NheI*) were linearized with the respective restriction enzymes, mentioned between parentheses, and transcribed using the T7 mMESSAGE-mACHINE transcription kit (Ambion, U.S.A.). hNa_v1.5/pcDNA3.1 (*XbaI*) was linearized with the respective restriction enzyme, mentioned between parentheses, and transcribed with the SP6 mMESSAGE-mACHINE transcription kit (Ambion, U.S.A.). Stage V and VI oocytes, harvested from anesthetized female *X. laevis* frogs as described previously, were injected with 30–50 nL of 1–3 μg/μL Na_v channel cRNA using a microinjector (Drummond Scientific, U.S.A.). The oocytes were then incubated in ND96 solution (in mM: NaCl 96, KCl 2, MgCl₂ 1, CaCl₂ 1.8, HEPES 5), adjusted to pH 7.5 and supplemented with 50 mg/L gentamycin sulfate and 90 mg/L theophylline at 16 °C for 1–5 days until the expression of ion channels.

2.2. Electrophysiological Characterization. Two-electrode voltage-clamp (TEVC) recordings were performed at room temperature using a GeneClamp 500 amplifier (Molecular Devices, Sunnyvale, California, U.S.A.) controlled by a pClamp data acquisition system (Molecular Devices). Whole-cell currents from oocytes were recorded 1–5 days after injection. Voltage and current electrodes were filled with 3 M KCl. The

Table 1. Modulatory Activities of Compounds 1–21 on Human Na_v1.3 and Na_v1.7 Isoforms

ID	Structure	IC ₅₀ ^a [μM]		ID	Structure	IC ₅₀ ^a [μM]	
		Na _v 1.3	Na _v 1.7			Na _v 1.3	Na _v 1.7
1		>30	27±6	12		24±8	>30
2		26±7	7±4	13		25±7	>30
3		25±7	19±8	14		>30	n.d. ^b
4		>30	15±4	15		>30	25±8
5		15±4	26±6	16		>30	9±5
6		>30	>30	17		>30	>30
7		24±9	26±5	18		>30	>30
8		25±8	26±8	19		>30	>30
9		>30	>30	20		>30	>30
10		>30	23±10	21		>30	>30
11		>30	>30	^a The concentration of compound that inhibits a sodium channel current by 50%. Each IC ₅₀ value is the mean of three independent experiments. ^b Not determined.			

resistances of both electrodes were kept between 0.7 and 1.7 MΩ. The elicited currents were sampled at 20 kHz and filtered at 2 kHz using a four-pole low-pass Bessel filter. To eliminate the effect of the voltage drop across the bath-grounding electrode, a two-electrode bath clamp actively controlled the bath potential. Leak subtraction was performed using a -P/4 protocol. For the electrophysiological characterization of the compounds 1–32, a number of voltage protocols were applied from a holding potential of -90 mV with a start-to-start pulse frequency of 0.2 Hz. Current traces were evoked in oocytes expressing the cloned Na_v channels according to the following protocol. From a holding potential of -90 mV, current traces were evoked by 100 ms depolarizations to the voltage corresponding to the maximal activation of the Na_v channel subtype in control conditions. All data were tested for normality using a D'Agustino Pearson omnibus normality

test. Data following a Gaussian distribution were analyzed for significance using one-way ANOVA, Bonferroni test. Non-parametric data were analyzed for significance using the Kruskal–Wallis, Dunn's test.

Compound Characterization. From both virtual screening campaigns (Figure 2), 32 compounds were selected and purchased from Enamine Ltd. The purities of compounds 2–5 and 16 with IC₅₀ values below 20 μM on human Na_v1.3 or Na_v1.7 were assessed using HPLC analyses on Agilent Technologies 1100 instrument with G1365B UV–vis detector, G1316A thermostat, and G1313A autosampler using Agilent Eclipse Plus C18 column (5 μm, 4.6 mm × 150 mm). Eluent consisted of 0.1% trifluoroacetic acid in water (A) and methanol (B). The gradient was 90% A to 10% A in 20 min, then 5 min 10% A, then 5 min to 90% A. HPLC purity of the active compounds 2–5 and 16 was above 95% monitored at

254 nm. ^1H NMR spectra of compounds **2–5** and **16** were recorded at 400 MHz on a Bruker AVANCE III spectrometer in $\text{DMSO}-d_6$ solution with TMS as an internal standard at 25 $^\circ\text{C}$, and their high resolution mass spectra were obtained using a VG-Analytical Autospec Q mass spectrometer (see Supporting Information for compound characterization data). The ^1H NMR and HRMS spectra confirmed the structures of compounds **2–5** and **16**.

RESULTS AND DISCUSSION

Ligand-Based Virtual Screening for Analogs of Compounds I and II. Clathrocin, a pyrrole-imidazole alkaloid from the marine sponge *Agelas clathrodes*, was identified as VGSC modulator.³⁵ Recently, we have designed and synthesized a library of conformationally restricted clathrocin analogs (Figure 1), some of which were found as state-dependent modulators of human $\text{Na}_v1.3$, $\text{Na}_v1.4$, or $\text{Na}_v1.7$ isoforms with IC_{50} values in the micromolar range.³⁶ Among the first clathrocin analogs synthesized, compound **I** (Figure 1) showed activity against $\text{Na}_v1.3$ and $\text{Na}_v1.7$ with IC_{50} values of 21 and 25 μM , respectively, while compound **II** (Figure 1) displayed 68% inactivated state I_{peak} block of $\text{Na}_v1.4$ at 10 μM . On the basis of these electrophysiological data, compounds **I** and **II** were selected as starting points for computer-aided discovery of improved analogs (Figure 2).

In the case of ROCS³⁷ 3D similarity search to find structural analogs of compound **I**, a hit list of 1000 highest ranked compounds, according to the TanimotoCombo score, was used for further analysis. These compounds were clustered by their functional-class fingerprints to enable selection of structurally diverse compounds from different clusters. A set of 21 commercially available compounds (Table 1) with the highest TanimotoCombo scores from the top ranked clusters was finally selected for biological evaluation for the modulation of human $\text{Na}_v1.3$ and $\text{Na}_v1.7$ isoforms and selectivity against the cardiac $\text{Na}_v1.5$ isoform.

Compounds identified in the ROCS ligand-based screening combined with fingerprint clustering in the case of compound **I** were structurally very similar. Most of them consisted of the central *meta* substituted phenyl ring, directly linked to a five-membered heterocyclic ring on one side and through amide bond to a bicyclic moiety on the other. Although in using this approach some compounds with improved activity were identified (Table 1), in the case of compound **II**, we decided to use structure-based virtual screening in a larger library resulting from ligand-based similarity searching to find $\text{Na}_v1.4$ blockers with more structural diversity. Therefore, an enriched library of 10,000 most similar compounds to compound **II** according to the TanimotoCombo score was further used in structure-based virtual screening using our human $\text{Na}_v1.4$ open-pore conformation homology model.

Structure-Based Virtual Screening of Enriched Library of Compound II Analogs. *Homology Modeling.* Until recently, structural interpretation of experimental data on VGSC was based on homology models, which were constructed by using crystal structures of the voltage-gated potassium channels as templates. In 2011, the first X-ray structure of bacterial VGSC from *Arcobacter butzleri* (Na_vAb) in a lipid-based bicelle system was determined at 2.7 Å resolution (Figure S4, Supporting Information).³ The channel was captured in its closed-pore conformation with four activated voltage sensors. This extremely important discovery was followed by determination of the X-ray structure of Na_vAb in two potentially

inactivated states:²⁵ structure of VGSC from *Rickettsiales* sp.²⁶ and finally, structure of the first open-pore conformation of VGSC from *Magnetococcus* sp. (Na_vMs).²⁷ These three-dimensional structures of bacterial VGSC enable building of human VGSC homology models of improved quality, which can be used for interpretation of experimental data and potentially for structure-based discovery of novel VGSC modulators.

There are important structural differences between the voltage-gated potassium and sodium channels based on their crystal structures. Unlike potassium channels, bacterial VGSC contain additional α -helix, named P2 helix, in the P-loop region between the selectivity filter residues and the S6 helices. Correct amino acid sequence alignment is of critical importance for building of an accurate homology model. The sequence similarity in transmembrane helices (S1–S6) between human and bacterial VGSC is higher than in their P-loop regions. On the basis of TTX binding data, Tikhonov and Zhorov⁴² proposed an adjusted sequence alignment in P2-helix, including deletions of residues three positions downstream from the selectivity filter residues (Figure S2, Supporting Information). Such modified sequence alignment stabilizes the P-region in the $\text{Na}_v1.4$ channel and allows building of the homology model that explains the available TTX binding data.⁴² Indeed, our homology model of human $\text{Na}_v1.4$, built based on Na_vAb as the template and new alignment in the P-loop region, allowed reproduction of the interactions between TTX and the channel (see below).⁵³

Because most of the small molecules interact with the voltage sensor or block the ion conduction pore,⁵⁴ we decided to build the S4–S6 part of the human skeletal muscle $\text{Na}_v1.4$ isoform. Our closed-pore human $\text{Na}_v1.4$ homology model, built based on Na_vAb as template (model 1), served as a basis for modeling of its open-pore conformation.

The first crystal structure of the voltage-gated sodium channel in its open-pore conformation (from *Magnetococcus* sp. (Na_vMs); PDB entry: 4F4L)²⁷ was not available at the time of construction of our human $\text{Na}_v1.4$ open-pore homology model, which we built based on the nonselective cation channel NaK from *Bacillus cereus*. The overlay of crystal structures of NaK in its closed-pore (PDB entry: 2AHY)⁴⁴ and open-pore (PDB entry: 3E86)⁴⁵ conformations (Figure S5, Supporting Information) revealed that the S5 helices (without M0 helix) and P-loops are almost identical. The most significant conformational changes occur in the S6 helices, at the gating hinge Gly residue (Figure S6, Supporting Information). In addition to simple bending at this residue, the pore lining helices also undergo a 45 $^\circ$ twist around their helical axis, which results in channel opening.⁴⁵ Considering the fact that the S5 helices and P-loops remain static during NaK channel gating, we proposed the same mechanism also for $\text{Na}_v1.4$. Thus, the S5–P-loop part of each repeat of the closed-pore model (model 1) was retained, while S6 helices were replaced by S6 helices modeled based on the NaK open-pore structure as the template (Figure S3, Supporting Information). Our open-pore homology model of $\text{Na}_v1.4$ (model 2) included the S5 and S6 helices and the P-loop between them because the voltage sensor S4 helices were not modeled due to their absence in the NaK open-pore structure.

Next, the obtained open-pore homology model was subjected to energy minimization to release steric clashes. The final structure was then used for geometrical quality assessment and evaluation by molecular docking of TTX and

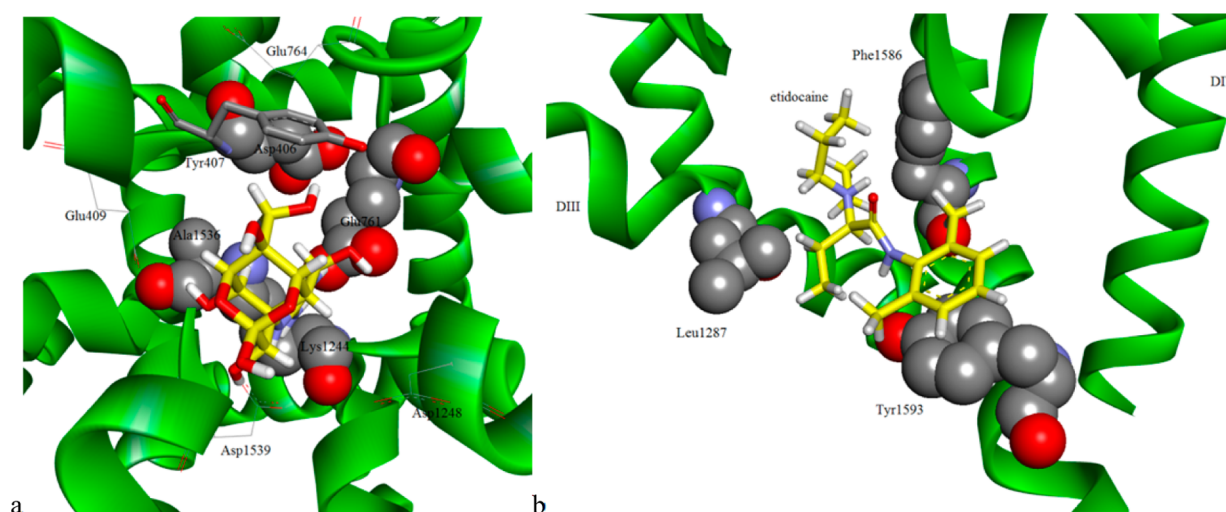


Figure 3. (a) Extracellular view of TTX binding mode in our human Na_v1.4 open-pore conformation homology model. DEKA motif residues are represented in CPK models. Tyr407 is represented in gray sticks, while outer carboxylates are represented as lines. TTX is represented in yellow sticks. (b) Etidocaine binding mode in our human Na_v1.4 open-pore conformation homology model. Local anesthetic-sensing residues are represented as CPK models, while etidocaine is represented in yellow sticks. Domains I and II are omitted for clarity.

Table 2. Modulatory Activities of Compounds 22–32 on Human Na_v1.4 Isoform

ID	Structure	Na _v 1.4 % inhibition at 10 μM ^a	ID	Structure	Na _v 1.4 % inhibition at 10 μM ^a
22		10.4	28		3.2
23		9.3	29		15.9
24		5.9	30		10.5
25		14.2	31		21.1
26		15.6	32		22.3
27		14.8	^aInactivated state I_peak block.		

local anesthetic etidocaine. The geometrical quality of the model was evaluated using Procheck.⁴⁹ Ramachandran plot analysis showed that the backbone dihedral angles of 100% of the amino acid residues were found in allowed regions, of which 96.4% were located in the most favored and 3.6% in additional allowed regions (Figure S8, Supporting Information).

Further, the model was evaluated by docking of TTX to the extracellular side of the channel pore and by docking of local anesthetic etidocaine to the central cavity of the channel. FlexX^{51,52} docking of TTX into the outer pore of the human Na_v1.4 open-pore homology model was able to reproduce experimental data on TTX binding. The toxin forms contacts

with the selectivity filter residues (DEKA motif) as well as with the outer carboxylates (Glu409, Glu764, Asp1248, and Asp1539), three positions downstream from the DEKA motif residues (Figure 3a; Figure S10, Supporting Information). The binding pose of TTX also reproduced the possible cation– π interaction between TTX guanidine group and Tyr407 side chain. Etidocaine was docked into the LA binding site in the inner pore of the human Na_v1.4 open-pore homology model. The FlexX-calculated binding mode of etidocaine is in agreement with experimental data^{55–57} and previous etidocaine binding mode studies.²⁸ The phenyl ring of etidocaine is in contact with Tyr1593, while alkyl chains of the molecule make hydrophobic interactions with Leu1287 and Phe1586, two LA

sensing residues (Figure 3b; Figure S11, Supporting Information). The dialkylammonium group of etidocaine is positioned in a way to form a proposed cation- π interaction with the side chain phenyl ring of Phe1586.

Because docking of TTX and etidocaine with FlexX was able to reproduce the experimental data on their binding, we concluded that the model was of suitable quality for structure-based virtual screening for novel Na_v1.4 modulators. All ligands obtained from the ligand-based similarity search in ROCS, using compound **II** as a query, were docked into the LA binding site in the inner pore of the channel, defined as in the case of etidocaine docking, and ranked according to the FlexX scoring function. Eleven highest ranked compounds (Table 2) were selected and obtained from Enamine Ltd. for biological testing.

Biological Activity. The activity of compounds **1–32** (Tables 1 and 2), possessing a predicted potential to block the human sodium channel isoforms Na_v1.3 and Na_v1.7 or Na_v1.4, was studied using automated patch clamp electrophysiology technique on the Sophion QPatch HT system. For Na_v1.3 and Na_v1.7 channels, the potency (IC₅₀) of test compounds was determined from concentration–response relationships established by cumulatively applying four escalating concentrations (0.3–10 μ M) of the test compound to a cell. For the Na_v1.4 channel, the efficacy (maximum inhibitory effect) of compounds was assessed in response to application of a single concentration (10 μ M) of each test compound as detailed in the Experimental section.

Analogues of Compound I. Modulation of ion permeation of human Na_v1.3 and Na_v1.7 by structurally similar compounds to **I** is presented in Table 1. The ZINC database we used for the 3D similarity search did not contain the query compounds and their analogs with retained 2-aminoimidazole moiety. In the series of pyrazole-containing compounds **1–8**, the most potent Na_v1.3 modulator was compound **5** with IC₅₀ value of 15 μ M, while compounds **2**, **3**, **7**, and **8** showed weaker activity (IC₅₀ values between 24 to 26 μ M) or were inactive (compounds **1**, **4**, and **6**). Thiazole derivatives **9** and **10**, triazole **11**, tetrazoles **14–17**, and structurally diverse compounds **18–21** were devoid of activity. The only weakly active nonpyrazole Na_v1.3 modulators were 1,3,4-oxadiazole **12** and tetrazole **13** with IC₅₀ values of 24 and 25 μ M, respectively. Screening of compounds **1–21** for their modulation of Na_v1.7 revealed better results compared to Na_v1.3 channels. Pyrazole **2** and tetrazole **16** with IC₅₀ values of 7 and 9 μ M, respectively, are among the most potent Na_v1.7 modulating clathrocin analogs discovered so far.^{35,36} Some activity was also displayed by pyrazoles **3** (IC₅₀ = 19 μ M) and **4** (IC₅₀ = 15 μ M), while compounds **1**, **5**, **7**, **8**, **10**, and **15** showed weaker activities (IC₅₀ values between 23 μ M and 27 μ M) or were completely inactive (compounds **6**, **9**, **11–13**, and **17–21** with IC₅₀ values >30 μ M). According to the electrophysiology data, all the active compounds act as state-dependent VGSC modulators that bind to the open-inactivated state but not to the closed resting state of Na_v1.3 or Na_v1.7 (IC₅₀ > 30 μ M). None of the compounds showed activity against cardiac Na_v1.5 isoform.

Analogues of Compound II. In contrast to the ligand-based virtual screening (ROCS similarity searching), selection of compounds based on docking of ROCS hits to the Na_v1.4 homology model gave a set of structurally more diverse compounds (Table 2). Eleven best scored compounds were purchased and tested for modulation of Na_v1.4. In comparison to the parent compound **II** (68% of inactivated state I_{peak}

block), all of them showed weaker activity with % of inactivated state I_{peak} block below 25% at 10 μ M. The most potent compound was pyrazole **32** with 22.3% inactivated state I_{peak} block of Na_v1.4. One reason for the low hit rate could be simply the small sample size, but in addition to this, template selection for the homology modeling of the open-pore conformation of human Na_v1.4 may be a factor. The recently determined crystal structure of the open-pore bacterial VGSC from *Magnetococcus* sp. (Na_vMs)²⁷ revealed that the mechanism of sodium channel opening in this case may differ from the mechanisms previously proposed for voltage-gated potassium and calcium channels. On the basis of the sequence of the first bacterial VGSC identified (NaChBac), the glycine residue in the middle of the S6 helix was proposed to act as a gating hinge.⁵⁸ However, the Na_vMs open-pore crystal structure suggests a different mechanism, which includes rotation of one residue in the middle of S6 helix, which swings S6 helix away from the central pore and enables the sodium ions to enter the cell through the open channel (Figure S7, Supporting Information).²⁷ The construction of our human Na_v1.4 open-pore homology model was based on the theory of glycine residue acting as a gating hinge (Figure S6, Supporting Information), and the NaK channel was used as a template to model the S6 helices (Figure S3, Supporting Information). Because in VGSC the mechanism of channel gating may be different, the template for our model building may not have been ideal and could have contributed to the low hit rate of the screening.

Compounds **1–32** were also tested for their activity against heterologously expressed Na_v1.3–Na_v1.5 and Na_v1.7 channels in *Xenopus laevis* oocytes. The results of these two electrode voltage clamp experiments corroborated well with the data obtained from the patch clamp experiments described above, although all active compounds showed lower activity compared with the mammalian cell system. However, because both results were obtained in different expression systems (patch clamp vs. voltage clamp), it is possible that these small differences can be explained as such. Because both systems use different cells to express channels, potential differences in post-translational modifications of the channels and differences in expression of the auxiliary subunits might influence pharmacology of the channels. Furthermore, differences in the membrane composition together with inherent differences in osmolarity of the recording solutions can provide an explanation for the differences observed between both expression systems.

CONCLUSION

In conclusion, inspired by the activity of some synthetic analogs of the marine pyrrole-imidazole alkaloid clathrocin, we have conducted virtual screening for potential human voltage-gated sodium channel modulators. Ligand-based similarity searching based on compound **I** combined with the cheminformatics tool of fingerprint clustering resulted in novel state-dependent modulators of Na_v1.3 and Na_v1.7 isoforms. Pyrazole **5** with an IC₅₀ value of 15 μ M displayed the highest affinity for Na_v1.3 among the 21 selected compounds, while pyrazole **2** (IC₅₀ = 7 μ M) and tetrazole **16** (IC₅₀ = 9 μ M) were found to be the most potent Na_v1.7 modulators, based on the clathrocin scaffold, discovered so far. On the basis of the electrophysiological data obtained for the selected 21 compounds, the 2-aminoimidazole moiety of compound **I** could be replaced by nitrogen-containing heterocycles (e.g., pyrazole, tetrazole, 1,2,4-oxadiazole, thiazole), while the indole moiety of **I** tolerates structurally diverse replacements (e.g. benzothiophene, benzofuran, benzi-

midazole). In the case of compound **II**, a combination of ligand- and structure-based virtual screening was employed for the discovery of Na_v1.4 modulators. Similarity search using compound **II** as a query was followed by docking of the enriched library to our homology model of the human Na_v1.4 isoform in open-pore conformation. Of the 11 structurally diverse compounds tested, none showed improved activity against Na_v1.4 compared to **II**. Although this might create an impression that cheminformatics tools are more efficient than virtual screening tools, it should be taken into consideration that the latter, besides being very sensitive to the protocol of homology modeling, involve also much more tunable controlling parameters than cheminformatics tools. In unfavorable combination, these factors may decrease the success of virtual screening tools. Additionally, the number of compound **II** analogs tested was smaller than the number of compounds similar to **I**, which might also be the reason for the lower hit rate of combined ligand- and structure-based protocol. Nevertheless, compounds **2** and **16** with promising Na_v1.7 modulatory activity represent new scaffolds for the design of novel state-dependent selective Na_v1.7 modulators.

■ ASSOCIATED CONTENT

■ Supporting Information

ROCS similarity search queries based on compounds **I** and **II**, sequence alignments, structures of templates used for homology modeling, Ramachandran plot, tetrodotoxin and etidocaine calculated binding poses, compound characterization data, and ¹H NMR spectra of compounds **2–5** and **16**. This material is available free of charge via the Internet at <http://pubs.acs.org>.

■ AUTHOR INFORMATION

Corresponding Author

*Phone: +386-1-4769561. Fax: +386-1-4258031. E-mail: daniel.kikelj@ffa.uni-lj.si.

Author Contributions

The manuscript was written through contributions of all authors. All authors have given approval to the final version of the manuscript.

Notes

The authors declare no competing financial interest.

■ ACKNOWLEDGMENTS

This work was supported by the Slovenian Research Agency (Grant No. P1-0208 and Grant No. Z1-5458) and the European Union FP7 Integrated Project MAREX: Exploring Marine Resources for Bioactive Compounds: From Discovery to Sustainable Production and Industrial Applications (Project No. FP7-KBBE-2009-3-245137).

■ ABBREVIATIONS

CNS, central nervous system; DS, Accelrys Discovery Studio; LA, local anesthetic; Na_vAb, voltage-gated sodium channel from *Arcobacter butzleri*; Na_vMs, voltage-gated sodium channel from *Magnetococcus* sp.; Na_v1.3, voltage-gated sodium channel 1.3 isoform; Na_v1.4, voltage-gated sodium channel 1.4 isoform; Na_v1.5, voltage-gated sodium channel 1.5 isoform; Na_v1.7, voltage-gated sodium channel 1.7 isoform; TTX, tetrodotoxin; VGSC, voltage-gated sodium channel

■ REFERENCES

- (1) Hodgkin, A. L.; Huxley, A. F. A quantitative description of membrane current and its application to conduction and excitation in nerve. *J. Physiol.* **1952**, *117*, 500–544.
- (2) Catterall, W. A. From ionic currents to molecular mechanisms: The structure and function of voltage-gated sodium channels. *Neuron* **2000**, *26*, 13–25.
- (3) Payandeh, J.; Scheuer, T.; Zheng, N.; Catterall, W. A. The crystal structure of a voltage-gated sodium channel. *Nature* **2011**, *475*, 353–358.
- (4) Catterall, W. A.; Goldin, A. L.; Waxman, S. G. International Union of Pharmacology. XLVII. Nomenclature and structure-function relationships of voltage-gated sodium channels. *Pharmacol. Rev.* **2005**, *57*, 397–409.
- (5) Goldin, A. L. Resurgence of sodium channel research. *Annu. Rev. Physiol.* **2001**, *63*, 871–894.
- (6) Andavan, G. S.; Lemmens-Gruber, R. Voltage-gated sodium channels: Mutations, channelopathies and targets. *Curr. Med. Chem.* **2011**, *18*, 377–397.
- (7) Lossin, C. A catalog of SCN1A variants. *Brain Dev.* **2009**, *31*, 114–130.
- (8) Heron, S. E.; Scheffer, I. E.; Berkovic, S. F.; Dibbens, L. M.; Mulley, J. C. Channelopathies in idiopathic epilepsy. *Neurotherapeutics* **2007**, *4*, 295–304.
- (9) Shi, X.; Yasumoto, S.; Nakagawa, E.; Fukasawa, T.; Uchiya, S.; Hirose, S. Missense mutation of the sodium channel gene SCN2A causes Dravet syndrome. *Brain Dev.* **2009**, *31*, 758–762.
- (10) Dib-Hajj, S. D.; Binshtok, A. M.; Cummins, T. R.; Jarvis, M. F.; Samad, T.; Zimmermann, K. Voltage-gated sodium channels in pain states: role in pathophysiology and targets for treatment. *Brain Res. Rev.* **2009**, *60*, 65–83.
- (11) Bendahhou, S.; Cummins, T. R.; Tawil, R.; Waxman, S. G.; Ptacek, L. J. Activation and inactivation of the voltage-gated sodium channel: Role of segment S5 revealed by a novel hyperkalaemic periodic paralysis mutation. *J. Neurosci.* **1999**, *19*, 4762–4771.
- (12) Heine, R.; Pika, U.; Lehmann-Horn, F. A novel SCN4A mutation causing myotonia aggravated by cold and potassium. *Hum. Mol. Genet.* **1993**, *2*, 1349–1353.
- (13) Benito, B.; Brugada, J.; Brugada, R.; Brugada, P. Brugada syndrome. *Rev. Esp. Cardiol.* **2009**, *62*, 1297–1315.
- (14) Goldenberg, I.; Zareba, W.; Moss, A. J. Long QT syndrome. *Curr. Probl. Cardiol.* **2008**, *33*, 629–694.
- (15) Ellinor, P. T.; Nam, E. G.; Shea, M. A.; Milan, D. J.; Ruskin, J. N.; MacRae, C. A. Cardiac sodium channel mutation in atrial fibrillation. *Heart Rhythm* **2008**, *5*, 99–105.
- (16) Clare, J. J.; Tate, S. N.; Nobbs, M.; Romanos, M. A. Voltage-gated sodium channels as therapeutic targets. *Drug Discovery Today* **2000**, *5*, 506–520.
- (17) Zuliani, V.; Patel, M. K.; Fantini, M.; Rivara, M. Recent advances in the medicinal chemistry of sodium channel blockers and their therapeutic potential. *Curr. Top. Med. Chem.* **2009**, *9*, 396–415.
- (18) Matulenko, M. A.; Scanio, M. J.; Kort, M. E. Voltage-gated sodium channel blockers for the treatment of chronic pain. *Curr. Top. Med. Chem.* **2009**, *9*, 362–376.
- (19) England, S.; de Groot, M. J. Subtype-selective targeting of voltage-gated sodium channels. *Br. J. Pharmacol.* **2009**, *158*, 1413–1425.
- (20) Fozzard, H. A.; Lee, P. J.; Lipkind, G. M. Mechanism of local anesthetic drug action on voltage-gated sodium channels. *Curr. Pharm. Des.* **2005**, *11*, 2671–2686.
- (21) Bregman, H.; Nguyen, H. N.; Feric, E.; Ligutti, J.; Liu, D.; McDermott, J. S.; Wilenkin, B.; Zou, A.; Huang, L.; Li, X.; McDonough, S. I.; Dimauro, E. F. The discovery of aminopyrazines as novel, potent Na_v1.7 antagonists: hit-to-lead identification and SAR. *Bioorg. Med. Chem. Lett.* **2012**, *22*, 2033–2042.
- (22) Bregman, H.; Berry, L.; Buchanan, J. L.; Chen, A.; Du, B.; Feric, E.; Hierl, M.; Huang, L.; Immke, D.; Janosky, B.; Johnson, D.; Li, X.; Ligutti, J.; Liu, D.; Malmberg, A.; Matson, D.; McDermott, J.; Miu, P.; Nguyen, H. N.; Patel, V. F.; Waldon, D.; Wilenkin, B.; Zheng, X. M.;

Zou, A.; McDonough, S. I.; DiMauro, E. F. Identification of a potent, state-dependent inhibitor of Na_v1.7 with oral efficacy in the formalin model of persistent pain. *J. Med. Chem.* **2011**, *54*, 4427–4445.

(23) Macsari, I.; Sandberg, L.; Besidski, Y.; Gravenfors, Y.; Ginman, T.; Bylund, J.; Bueters, T.; Eriksson, A. B.; Lund, P. E.; Venyike, E.; Arvidsson, P. I. Phenyl isoxazole voltage-gated sodium channel blockers: structure and activity relationship. *Bioorg. Med. Chem. Lett.* **2011**, *21*, 3871–3876.

(24) Ilyin, V. I.; Pomonis, J. D.; Whiteside, G. T.; Harrison, J. E.; Pearson, M. S.; Mark, L.; Turchin, P. I.; Gottshall, S.; Carter, R. B.; Nguyen, P.; Hogenkamp, D. J.; Olanrewaju, S.; Benjamin, E.; Woodward, R. M. Pharmacology of 2-[4-(4-chloro-2-fluorophenoxy)-phenyl]-pyrimidine-4-carboxamide: A potent, broad-spectrum state-dependent sodium channel blocker for treating pain states. *J. Pharmacol. Exp. Ther.* **2006**, *318*, 1083–1093.

(25) Payandeh, J.; Gamal El-Din, T. M.; Scheuer, T.; Zheng, N.; Catterall, W. A. Crystal structure of a voltage-gated sodium channel in two potentially inactivated states. *Nature* **2012**, *486*, 135–139.

(26) Zhang, X.; Ren, W.; DeCaen, P.; Yan, C.; Tao, X.; Tang, L.; Wang, J.; Hasegawa, K.; Kumasaka, T.; He, J.; Clapham, D. E.; Yan, N. Crystal structure of an orthologue of the NaChBac voltage-gated sodium channel. *Nature* **2012**, *486*, 130–134.

(27) McCusker, E. C.; Bagnieris, C.; Naylor, C. E.; Cole, A. R.; D'Avanzo, N.; Nichols, C. G.; Wallace, B. A. Structure of a bacterial voltage-gated sodium channel pore reveals mechanisms of opening and closing. *Nat. Commun.* **2012**, *3*, 1102.

(28) Lipkind, G. M.; Fozzard, H. A. Molecular modeling of local anesthetic drug binding by voltage-gated sodium channels. *Mol. Pharmacol.* **2005**, *68*, 1611–1622.

(29) Pirard, B.; Brendel, J.; Peukert, S. The discovery of Kv1.5 blockers as a case study for the application of virtual screening approaches. *J. Chem. Inf. Model.* **2005**, *45*, 477–485.

(30) Al-Sabi, A.; McArthur, J.; Ostroumov, V.; French, R. Marine toxins that target voltage-gated sodium channels. *Mar. Drugs* **2006**, *4*, 157–192.

(31) Forte, B.; Malgesini, B.; Piutti, C.; Quartieri, F.; Scolaro, A.; Papeo, G. A submarine journey: The pyrrole-imidazole alkaloids. *Mar. Drugs* **2009**, *7*, 705–753.

(32) Al-Mourabit, A.; Zancanella, M. A.; Tilvi, S.; Romo, D. Biosynthesis, asymmetric synthesis, and pharmacology, including cellular targets, of the pyrrole-2-aminoimidazole marine alkaloids. *Nat. Prod. Rep.* **2011**, *28*, 1229–1260.

(33) Rentas, A. L.; Rosa, R.; Rodriguez, A. D.; De Motta, G. E. Effect of alkaloid toxins from tropical marine sponges on membrane sodium currents. *Toxicon* **1995**, *33*, 491–497.

(34) Bickmeyer, U.; Drechsler, C.; Kock, M.; Assmann, M. Brominated pyrrole alkaloids from marine *Agelas* sponges reduce depolarization-induced cellular calcium elevation. *Toxicon* **2004**, *44*, 45–51.

(35) Hodnik, Ž.; Tomašić, T.; Peterlin Mašič, L.; Chan, F.; Kirby, R. W.; Madge, D. J.; Kikelj, D. Novel state-dependent voltage-gated sodium channel modulators, based on marine alkaloids from *Agelas* sponges. *Eur. J. Med. Chem.* **2013**, *70*, 154–164.

(36) Zidar, N.; Jakopin, Ž.; Madge, D. J.; Chan, F.; Tytgat, J.; Peigneur, S.; Sollner Dolenc, M.; Tomašić, T.; Ilaš, J.; Peterlin Mašič, L.; Kikelj, D. Substituted 4-phenyl-2-aminoimidazoles and 4-phenyl-4,5-dihydro-2-aminoimidazoles as voltage-gated sodium channel modulators. **2013**, submitted.

(37) Grant, J. A.; Gallardo, M. A.; Pickup, B. T. A fast method of molecular shape comparison: A simple application of a Gaussian description of molecular shape. *J. Comput. Chem.* **1996**, *17*, 1653–1666.

(38) Irwin, J. J.; Shoichet, B. K. ZINC-a free database of commercially available compounds for virtual screening. *J. Chem. Inf. Model.* **2005**, *45*, 177–182.

(39) Accelrys Discovery Studio 3.0. Accelrys, Inc. <http://accelrys.com/products/discovery-studio/visualization-download.php>.

(40) LeadIT version 2.1.3. BioSolve IT (GmbH). <http://www.biosolveit.de/LeadIT/index.html?ct=1>.

(41) Hawkins, P. C.; Skillman, A. G.; Warren, G. L.; Ellingson, B. A.; Stahl, M. T. Conformer generation with OMEGA: algorithm and validation using high quality structures from the Protein Databank and Cambridge Structural Database. *J. Chem. Inf. Model.* **2010**, *50*, 572–584.

(42) Tikhonov, D. B.; Zhorov, B. S. Architecture and pore block of eukaryotic voltage-gated sodium channels in view of Na_vAb bacterial sodium channel structure. *Mol. Pharmacol.* **2012**, *82*, 97–104.

(43) Sali, A.; Blundell, T. L. Comparative protein modelling by satisfaction of spatial restraints. *J. Mol. Biol.* **1993**, *234*, 779–815.

(44) Shi, N.; Ye, S.; Alam, A.; Chen, L.; Jiang, Y. Atomic structure of a Na⁺- and K⁺-conducting channel. *Nature* **2006**, *440*, 570–574.

(45) Alam, A.; Jiang, Y. High-resolution structure of the open NaK channel. *Nat. Struct. Mol. Biol.* **2009**, *16*, 30–34.

(46) Chakrapani, S.; Sompornpisut, P.; Intharathep, P.; Roux, B.; Perozo, E. The activated state of a sodium channel voltage sensor in a membrane environment. *Proc. Natl. Acad. Sci. U.S.A.* **2010**, *107*, 5435–5440.

(47) Brooks, B. R.; Brucoleri, R. E.; Olafson, B. D.; States, D. J.; Swaminathan, S.; Karplus, M. Charmm - a program for macromolecular energy, minimization, and dynamics calculations. *J. Comput. Chem.* **1983**, *4*, 187–217.

(48) Spassov, V. Z.; Yan, L.; Szalma, S. Introducing an implicit membrane in generalized Born/solvent accessibility continuum solvent models. *J. Phys. Chem. B* **2002**, *106*, 8726–8738.

(49) Laskowski, R. A.; Macarthur, M. W.; Moss, D. S.; Thornton, J. M. Procheck - a program to check the stereochemical quality of protein structures. *J. Appl. Crystallogr.* **1993**, *26*, 283–291.

(50) Halgren, T. A. Merck molecular force field. 1. Basis, form, scope, parameterization, and performance of MMFF94. *J. Comput. Chem.* **1996**, *17*, 490–519.

(51) Rarey, M.; Kramer, B.; Lengauer, T.; Klebe, G. A fast flexible docking method using an incremental construction algorithm. *J. Mol. Biol.* **1996**, *261*, 470–489.

(52) Rarey, M.; Wefing, S.; Lengauer, T. Placement of medium-sized molecular fragments into active sites of proteins. *J. Comput.-Aided Mol. Des.* **1996**, *10*, 41–54.

(53) Fozzard, H. A.; Lipkind, G. M. The tetrodotoxin binding site is within the outer vestibule of the sodium channel. *Mar. Drugs* **2010**, *8*, 219–234.

(54) Stevens, M.; Peigneur, S.; Tytgat, J. Neurotoxins and their binding areas on voltage-gated sodium channels. *Front. Pharmacol.* **2011**, *2*, 71.

(55) Ragsdale, D. S.; McPhee, J. C.; Scheuer, T.; Catterall, W. A. Molecular determinants of state-dependent block of Na⁺ channels by local anesthetics. *Science* **1994**, *265*, 1724–1728.

(56) Yarov-Yarovoy, V.; Brown, J.; Sharp, E. M.; Clare, J. J.; Scheuer, T.; Catterall, W. A. Molecular determinants of voltage-dependent gating and binding of pore-blocking drugs in transmembrane segment IIS6 of the Na⁺ channel alpha subunit. *J. Biol. Chem.* **2001**, *276*, 20–27.

(57) Yarov-Yarovoy, V.; McPhee, J. C.; Idsvoog, D.; Pate, C.; Scheuer, T.; Catterall, W. A. Role of amino acid residues in transmembrane segments IS6 and IIS6 of the Na⁺ channel alpha subunit in voltage-dependent gating and drug block. *J. Biol. Chem.* **2002**, *277*, 35393–35401.

(58) Zhao, Y.; Yarov-Yarovoy, V.; Scheuer, T.; Catterall, W. A. A gating hinge in Na⁺ channels; a molecular switch for electrical signaling. *Neuron* **2004**, *41*, 859–865.